Control co-design for wave energy farms: Optimisation of array layout and mooring configuration in a realistic wave climate

Control Co-Design for Wave Energy Farms: Optimisation of Array Layout and Mooring Configurations in a Realistic Wave Climate

Yerai Peña-Sanchez[a,*], Demián García-Violini[b,c,d], Markel Penalba[a,e], Ander Zarketa-Astigarraga[a], Francesco Ferri[f], Vincenzo Nava[g,h], John V. Ringwood[d]

[a] *Fluid Mechanics Department, Mondragon University, Loramendi 4, 20500 Arrasate, Spain*
[b] *Departamento de Ciencia y Tecnología, Universidad Nacional de Quilmes, Roque Saenz Peña 352, Bernal B1876, Argentina*
[c] *Consejo Nacional de Investigaciones Científicas y Técnicas (CONICET), Argentina*
[d] *Centre for Ocean Energy Research, Maynooth University, Maynooth, Ireland*
[e] *Ikerbasque, Basque Foundation for Science, Euskadi Plaza 5, 48011 Bilbao, Spain*
[f] *Department of the Built Environment, Aalborg University, Aalborg, Denmark*
[g] *Basque Center for Applied Mathematics (BCAM), Mazarredo Zumarkalea 14, Bilbao, Spain*
[h] *TECNALIA, Basque Research and Technology Alliance (BRTA), Astondo Bidea, Edificio 700, Derio, 48160, Spain*

Abstract

This paper presents a novel Control Co-Design (CCD) methodology aimed at economically optimising the layout of wave energy converter (WEC) arrays. CCD ensures the synergy of optimised WEC and array parameters with the final control strategy, resulting in a comprehensive and efficient design of the array. By integrating a spectral-based control strategy into the array layout design, this study pursues the twin objectives of maximising energy absorption while reducing costs. To prove the performance of the proposed methodology, an application case considers an array of five realistic devices deployed in-line on a realistic testing site, with different spacing, alignment, and mooring arrangements. Energy capture and system cost evaluations are conducted, with results emphasising the significance of incorporating advanced control strategies in the design phase to improve energy absorption and reduce costs.

Keywords: Wave energy, Wave farms, Control Co-Design, Mooring lines, Optimisation, Techno-economics

1. Introduction

In the pursuit of a sustainable, carbon-neutral global energy system, a significant expansion of renewable energy sources is paramount, marking a vital step away from fossil fuels. This transition aligns with the objectives outlined in both the Paris Agreement [1] and the latest assessment by the Intergovernmental Panel on Climate Change (IPCC) [2], aiming to mitigate the severe impacts of climate change [3]. Wind and solar energy technologies are already mature and reliable, but the massive upscaling to expedite this transition effectively will require the support of additional and diverse sources of energy. For example, the International Renewable Energy Agency (IRENA) estimates a staggering 14 TW increase in global renewable energy installed capacity requirement by 2050 [4]. This underlines the sheer magnitude of the challenge, for which the International Energy Agency predicts that roughly 45% of CO_2 emissions reduction by 2050 will be attributed to technologies still in the developmental stage [5]. In this context, offshore renewable energy (ORE) technologies, from floating offshore wind to tidal and wave technologies, emerge as a promising alternative. Wave and tidal energy, though in early stages of development, are anticipated to make substantial contributions to the future energy mix [6, 7]. The ambition of wave/tidal technologies is to achieve over 300 GW of installed, saving 500 Mt of carbon emission by 2050.

The potential of ocean waves is enormous, but wave energy technology is still unprepared for its commercialisation, with all the currently existing projects (about 2.5 MW of total installed capacity

*Corresponding author
Email address: ypena@mondragon.edu (Yerai Peña-Sanchez)

worldwide) targeting research and demonstration [8]. Hence, at the current state of development, one can say that wave power is expected to have a different role in the energy mix, such as providing energy to isolated islands with microgrids currently powered by diesel generators [9] or supplying a more reliable, less variable and more predictable energy source [10, 11]. In addition, compared to other renewable resources, wave energy has an advantage in predictability [12].

The future of wave energy predominantly hinges on wave energy converter (WEC) arrays, considering, among others, the limited power output of individual devices, the economies of scale in operation and maintenance (O&M) requirements [13]. In addition, IRENA has recently published a set of recommendations to enable the economic viability of wave energy, encouraging larger deployments that will enable significant cost reductions (to about 100€/MWh) [14]. Nowadays, key research and development efforts are mostly directed towards optimising the size and arrangement of these WEC arrays [8]. Despite extensive analysis of array layout optimisation in existing literature, many questions in this domain remain unanswered. Furthermore, there is a need for a thorough exploration of various associated aspects including, but not limited to, the interconnection of electrical cables and mooring lines, as well as the efficient management of O&M tasks.

Commonly, the optimisation of WEC arrays in the literature focuses on layout optimisation based on pure hydrodynamic optimisation [15, 16], with the aim of maximising the constructive interaction among the devices or minimising the destructive interaction. Given the high computational cost of simulation with several WECs, different approaches from analytical to numerical to experimental methods [15] have been employed. Early array layout optimisation studies used analytical and semi-analytical approaches based on the small-body approximation [17], or the plane-wave approximation [18], which are demonstrated to perform well at low and high frequencies, respectively [19]. The computational efficiency of these (semi-)analytical models enables the analysis of large arrays of up to 1000 devices [20] or multi-directional studies [21].

Similar studies have also been carried out using numerical models, although limited by the computational cost. One of the most common approaches, based on numerical models, is using boundary element method (BEM) solvers, such as NEMOH [22] and WAMIT [23]. Such models consider the effects of both the diffracted and radiated wave fields within the array. However, these numerical models are computationally expensive, especially with relatively large arrays. Overall, other than for optimisation purposes, numerical models have been used to characterise the performance of WEC arrays, from the analysis of basic hydrodynamic interaction effects as a function of the inter-device distance [24] to the assessment of different array sizes and layouts in realistic wave climates [25, 26, 27]. Finally, analytical and numerical models are complemented with experimental studies [28, 29, 30, 31, 32], which are usually restricted to relatively small sizes, for obvious reasons. In summary, analytical, numerical, and experimental methods have been suggested for the assessment of the hydrodynamic performance of WEC arrays.

However, the hydrodynamic performance of WEC arrays is often evaluated either under uncontrolled [24] or passive control conditions [25, 26, 27], resulting in under-excited WECs for which the hydrodynamic interaction effects are relatively mild. Garcia-Rosa et al. [16] demonstrate that the behaviour of individual WECs under different control techniques can greatly influence the expected hydrodynamic interaction between devices, potentially shifting destructive interactions into constructive ones. This has a substantial impact on the overall performance of the array, underscoring the importance of carefully considering the control strategy in WEC array layout design. Traditionally, the control strategy stage comes into play after the device and the WEC array layout have been optimised to maximise energy extraction. However, this optimisation process does not guarantee that all aspects of the WECs or WEC arrays are optimal since the implementation of advanced control strategies significantly alters the WEC motion. The mismatch between the behaviour of the (optimised) WEC design and the behaviour when considering advanced control is addressed by applying design constraints to the controller, which may lead to sub-optimal results [33]. To address such a challenge, control co-design (CCD) [34] of WECs or WEC arrays [35], where energy maximising control strategies are incorporated into the optimisation loop from the early stages, has recently gained popularity as a more integrative approach. In other words, this design paradigm emphasises a *control-informed* optimisation approach. Several studies in the literature have demonstrated the benefits of

CCD for the optimisation of different WEC-related parameters. For example, [35] highlights that CCD strategies contribute significantly to achieving an optimal structural design for the absorber geometry, aligning it with the energy-maximising control scheme. Another interesting example is [36], where the authors optimise the PTO configuration considering a spectral-control technique.

Regardless of the selected modelling approach and control strategy, the hydrodynamic performance of WEC arrays, considering interaction effects among the devices in the array, is commonly quantified by means of the q-factor. This factor compares the total energy absorbed by the entire array (E_{array}) to the energy absorption of the same number of isolated devices:

$$\mathrm{q} = \frac{E_{array}}{n_{\mathrm{b}} E_{\mathrm{isol}}}, \tag{1}$$

where E_{isol} is the energy absorbed by an isolated device and n_{b} the number of bodies composing the array. Hence, the q-factor can yield q$>$ 1, q$=$ 1, or q$<$ 1, inferring constructive, neutral and destructive hydrodynamic interactions.

However, several authors show a level of scepticism about whether constructive effects are realistic [37, 38, 39]. Although specific separation between devices can theoretically lead to constructive hydrodynamic interaction, the q-factor alone is not expected to exclusively determine the optimal design of array layouts, since this will be mostly influenced by significant cost factors such as moorings and electrical interconnection. Yet, these two aspects are commonly neglected in the literature when the optimisation of a WEC array is considered. Shared mooring lines in WEC arrays are studied for different types of device array size and layouts and mooring configurations: 8 heaving two-body point-absorber devices interconnected employing the KARRATU mooring configuration [40], 5 floating oscillating water column WECs interconnected via four different shared mooring configurations [30] and 6 heaving point-absorbers in a hexagon shape array layout [41]. Economic aspects are considered in [30, 41], but no optimisation is performed. In contrast, the optimisation of mooring lines is considered in [42], but a single device is considered. Finally, none of the mentioned studies considers advanced control strategies for the WEC array.

Hence, to the best of the authors' knowledge, a preliminary study by the same authors [43] is the only study in the literature that considers a control-informed optimisation which couples array layouts and mooring systems, including shared mooring configurations, from an economic perspective. However, [43] considers a simplified case study with only three WECs, a single array layout and a single panchromatic sea state (H_s =2.5m & T_p =10s). The present paper significantly extends the CCD framework for WEC arrays presented in [43] by (i) increasing the size of the WEC array to include 5 devices as suggested in [27], (ii) studying different array configurations, (iii) considering a realistic wave climate with all the relevant sea states, and (iv) incorporating a realistic mooring configuration following the KARRATU concept suggested in [40].

The remainder of the paper is laid out as follows: Section 2 describes the WEC array numerical model employed in this study, along with the introduction of the tool considered to compute the hydrodynamic parameters of the WEC arrays; Sections 3 and 4 outline the spectral control method, defining the objective function and the CCD strategy, respectively; Section 5 introduces the considered case study; Section 6 illustrates the most relevant results, and Section 7 draws the main conclusions of the study.

2. WEC Array Hydrodynamic Model

In this section, the considered dynamic model of the WEC array, which accounts for the interactions between the fluid (water) and the floating bodies, is introduced. This model also considers interactions between various bodies due to the radiated and diffracted waves originating from the other devices in the array. Thus, the model is formulated, in the time-domain, based on Newton's second law, as follows:

$$(m + \mu_\infty)\,\ddot{x}(t) = f_{\mathrm{e}}(t) - f_{\mathrm{h}}(t) - f_{\mathrm{r}}(t) - f_{\mathrm{m}}(t) - f_{\mathrm{u}}(t), \tag{2}$$

where the mass matrix $m \in \mathbb{R}^{n_{\mathrm{b}} \times n_{\mathrm{b}}}$ holds the mass of each device on its diagonal, with zeros elsewhere. The infinite frequency added mass of the WECs, denoted as $\mu_\infty \in \mathbb{R}^{n_{\mathrm{b}} \times n_{\mathrm{b}}}$, encompasses both the diagonal elements representing the infinite frequency added mass of the individual WECs and the off-diagonal elements accounting for the interactions. The state vectors, $x(t) \in \mathbb{R}^{n_{\mathrm{b}}}$, $\dot{x}(t) \in \mathbb{R}^{n_{\mathrm{b}}}$ (or equivalently, $v(t)$), and $\ddot{x}(t) \in \mathbb{R}^{n_{\mathrm{b}}}$ (or equivalently, $a(t)$), contain information about the position, velocity, and acceleration of the WECs, respectively.

The forces acting on the WECs, as introduced in Equation (2), encompass several components:

- the hydrostatic force $f_{\mathrm{r}}(t)$, which arises from buoyancy and gravity forces, is represented as $S_{\mathrm{h}}x(t)$, with $S_{\mathrm{h}} \in \mathbb{R}^{n_{\mathrm{b}} \times n_{\mathrm{b}}}$ being the hydrostatic stiffness matrix;
- the radiation force, originating from waves radiated due to WEC motion, is calculated using a convolution integral as $f_{\mathrm{r}}(t) = k_{\mathrm{r}_{i,j}}(t) * \dot{x}_j(t)$, where $k_{\mathrm{r}}(t)$ denotes the radiation convolution kernel;
- the mooring force, modelled as a spring-damper system, is expressed as $f_{\mathrm{m}}(t) = k_{\mathrm{m}}x(t) + b_{\mathrm{m}}\dot{x}(t)$, where $k_{\mathrm{m}} \in \mathbb{R}^{n_{\mathrm{b}} \times n_{\mathrm{b}}}$ and $b_{\mathrm{m}} \in \mathbb{R}^{n_{\mathrm{b}} \times n_{\mathrm{b}}}$ represent the mooring stiffness and damping matrices;
- and the wave excitation force and the PTO control force are defined as $f_{\mathrm{e}}(t) \in \mathbb{R}^{n_{\mathrm{b}}}$ and $f_{\mathrm{u}}(t) \in \mathbb{R}^{n_{\mathrm{b}}}$, respectively.

It is important to note that both the infinite frequency added mass matrix (μ_∞) and the radiation convolution kernel matrix (k_{r}) can be calculated based on the frequency-domain radiation added-mass and damping hydrodynamic coefficients ($A_{\mathrm{r}}(\omega) \in \mathbb{R}^{n_{\mathrm{b}} \times n_{\mathrm{b}}}$ and $B_{\mathrm{r}}(\omega) \in \mathbb{R}^{n_{\mathrm{b}} \times n_{\mathrm{b}}}$) using Ogilvie's relations [44] as follows:

$$\begin{aligned} A_{\mathrm{r}}(\omega) &= \mu_\infty - \tfrac{1}{\omega}\int_0^{+\infty} k_{\mathrm{r}}(t)\sin(\omega t)dt, \\ B_{\mathrm{r}}(\omega) &= \int_0^{+\infty} k_{\mathrm{r}}(t)\cos(\omega t)dt. \end{aligned} \tag{3}$$

Similarly, the radiation convolution kernel k_{r} can be defined in the frequency-domain, denoted by uppercase letters for frequency-domain variables, as

$$K_{\mathrm{r}}(\omega) = B_{\mathrm{r}}(\omega) + \jmath\omega\left[A_{\mathrm{r}}(\omega) - \mu_\infty\right]. \tag{4}$$

Therefore, Equation (2) can now be defined in the frequency-domain using the force-to-velocity description of the array [45] as:

$$V(\omega) = Z_i^{-1}(\omega)\left[F_{\mathrm{e}}(\omega) - F_{\mathrm{u}}(\omega)\right], \tag{5}$$

where $Z_i(\omega) \in \mathbb{I}^{n_{\mathrm{b}} \times n_{\mathrm{b}}}$ is the intrinsic impedance of the system, which can be defined as follows:

$$Z_i(\omega) = B_{\mathrm{r}}(\omega) + b_{\mathrm{m}} + \jmath\omega\left(m + A_{\mathrm{r}}(\omega) - \frac{s_{\mathrm{h}} + s_{\mathrm{m}}}{\omega^2}\right). \tag{6}$$

The force-to-velocity transfer function [46], essential for control design purposes, can now be defined based on Equation (6) as

$$\begin{aligned} G_{\mathrm{fv}}(\omega) = \jmath\omega[&- \omega^2(m + \mu_\infty) + \jmath\omega(H_{\mathrm{r}}(\omega) + b_{\mathrm{m}}) + \\ &+ s_{\mathrm{h}} + s_{\mathrm{m}}]^{-1}. \end{aligned} \tag{7}$$

Note that all the frequency-domain hydrodynamic parameters required for the calculation of $H_{\mathrm{r}}(\omega)$, denoted as $A_{\mathrm{r}}(\omega)$ and $B_{\mathrm{r}}(\omega)$, along with the excitation force parameters required for establishing the relationship between wave elevation and excitation force, represented as $\mathcal{H}_{\mathrm{e}}(\omega)$,

$$F_e(\omega) = \mathcal{H}_{\mathrm{e}}(\omega)\eta(\omega), \tag{8}$$

with $\eta(\omega)$ representing the free surface, can be determined using BEM solvers.

Boundary element methods have the advantage of being able to cope with a 3D formulation of the hydrodynamic problem, which allows the calculation of any WEC geometry. However, they become too computationally expensive when dealing with many interacting WECs. On the other hand, Kagemoto and Yue [47] came up with a direct matrix method approach, comparable to BEM codes in terms of capabilities and accuracy of the results, which significantly reduces the computation time. Such an approach was later combined with results from conventional BEM software, allowing the solution for WECs of any shape and mode of operation [48]. In particular, to reduce the computational effort for large arrays, the direct matrix method estimates the wave field for each WEC as a summation of the undisturbed incident wave field plus the wave scattered and radiated by other devices in the array.

These array effects are modelled using partial waves whose amplitude is obtained by fitting the velocity potential of the device obtained by BEM software. In general, for simple WEC geometries, only a few partial waves are sufficient to reproduce the wave field accurately while, for complex geometries, 10 or 20 partial waves are needed. To this extent, the hydrodynamic effect of a single body is fully represented by few partial waves, compared to a standard BEM where the hydrodynamic effects are estimated from the amplitude of the source potential, which has to be solved for each mesh node (with hundreds to thousands of elements). Hence, a version of the BEM solver NEMOH [22], including the direct matrix method for WEC arrays, is considered here to compute the hydrodynamic parameters of all the analysed cases.

3. Spectral control

This section offers an overview of the spectral control strategy implemented in this study. In essence, spectral controllers are control schemes designed to optimise the control input, with respect to a specific objective function. They rely on a direct transcription method that represents the system variables using a suitable set of basis functions. Spectral controllers excel in managing physical constraints and can theoretically achieve optimal solutions (based on the chosen resolution of the basis functions) [49], with reduced computation complexity compared to, say, MPC [50]. In the context of this study, a spectral-based controller is employed to ensure optimal power capture, while accounting for realistic motion and PTO force limitations. For a deeper understanding, Sections 3.1 and 3.2 delve into the general control objectives for WECs and the fundamental principles of spectral controllers, respectively.

3.1. WEC control objective function

As mentioned in the introduction, the main goal of a WEC control problem is to maximise the total absorbed energy. For the case of a WEC array system, subject to an external excitation force $f_{\mathrm{e}}(t)$ and controlled by a PTO force $f_{\mathrm{u}}(t)$, the total absorbed energy for all devices in the array ($E \in \mathbb{R}$) over the time interval $[0, T]$ can be computed as follows:

$$E = -\int_0^T P(t)dt = -\int_0^T \dot{x}^{\intercal}(t) f_{\mathrm{u}}(t)dt, \tag{9}$$

where $P(t) \in \mathbb{R}$ is the (instantaneous) absorbed power. Thus, the control problem is commonly expressed as

$$\begin{aligned} \max_{f_{\mathrm{u}}(t)} \quad & -\int_0^T \dot{x}(t)^{\intercal} f_{\mathrm{u}}(t)dt \\ \text{subject to} \quad & \begin{cases} \dot{\mathrm{x}} = \mathcal{F}(\mathrm{x}, f_{\mathrm{u}}, f_{\mathrm{e}}) \\ \dot{x} = \mathcal{G}(\mathrm{x}) \\ \mathcal{C} \end{cases} \end{aligned} \tag{10}$$

with $\mathcal{F}(x, f_{\mathrm{u}}, f_{\mathrm{e}})$ representing the multiple-input multiple-output (MIMO) state-space system of the WEC, derived from Equation (2), $\mathcal{G}(\mathrm{x})$ the output mapping of the state space, where $\mathrm{x} \mapsto \dot{x}$, and the set of considered constraints, denoted as $\mathcal{C}$, is limited to displacement and PTO force constraints, specifically $x_{\min} \leq x(t) \leq x_{\max}$ and $f_{\min} \leq f_{\mathrm{u}}(t) \leq f_{\max}$, respectively.

3.2. Spectral control

In this study, a control methodology that relies on (pseudo-)spectral techniques is explored to tackle the control problem outlined in Equation (10). The initial step entails discretising the optimal control formulation derived from Equation (10) within the spectral domain. This discretisation procedure involves projecting the state vector $x(t)$ and the control force f_{u} onto an orthonormal vector space with a dimension of N, which is achieved through a linear combination of orthogonal basis functions, denoted as $\Phi = [\phi_1, \phi_2, \cdots, \phi_N]$. Among the potential choices for these basis functions, the Fourier basis is a pertinent selection, inspired by the harmonic characteristics of the WEC variables. Consequently, the approximation of the states and control force takes the form of:

$$\begin{aligned} x(t) &\approx \mathrm{x}^N(t) = \hat{\mathrm{x}}\Phi(t)^{\intercal}, \\ f_{\mathrm{u}}(t) &\approx \mathrm{f}_{\mathrm{u}}^N(t) = \hat{\mathrm{f}}_{\mathrm{u}}\Phi(t)^{\intercal}, \end{aligned} \tag{11}$$

with both coefficient vectors $\hat{\mathrm{x}} = [\hat{x}_1, \hat{x}_2, \cdots, \hat{x}_N]$ and $\hat{\mathrm{f}}_{\mathrm{u}} = [\hat{f}_{\mathrm{u}1}, \hat{f}_{\mathrm{u}2}, \cdots, \hat{f}_{\mathrm{u}N}]$ as elements of the real vector space $\mathbb{R}^{n_{\mathrm{b}} \times N}$. Considering such a (pseudo-) spectral framework, the WEC array equation of motion introduced in Section 2 can be approximated [51] as follows:

$$\hat{\mathrm{v}} = (\hat{\mathrm{f}}_{\mathrm{e}} - \hat{\mathrm{f}}_{\mathrm{u}})\mathrm{G}_{\mathrm{o}}. \tag{12}$$

In Equation (12), the coefficient vector $\hat{\mathrm{v}} = [v_1, v_2, \cdots, v_N]^{\intercal}$ serves as an approximation for the velocities of the WECs in the array $\mathrm{v}(t)$, while G_{o} denotes the force-to-velocity system model. Furthermore, $\hat{\mathrm{f}}\mathrm{e} = [\hat{f}_{\mathrm{e}1}, \hat{f}_{\mathrm{e}2}, \cdots, \hat{f}_{\mathrm{e}N}]^{\intercal}$ represents the coefficient set $\hat{f}_{\mathrm{e}1}, \hat{f}_{\mathrm{e}2}, \cdots, \hat{f}_{\mathrm{e}N}$ utilised to approximate the excitation forces affecting the different WECs.

Then, considering the mathematical properties of the basis functions Φ_j [52], one can approximate the objective function in Equation (9) as

$$E \approx J_N = \int_0^T \hat{\mathrm{f}}_{\mathrm{u}}\Phi(t)^{\intercal}\Phi(t)\hat{\mathrm{v}}^{\intercal} = -\frac{T}{2}\hat{\mathrm{f}}_{\mathrm{u}}\hat{\mathrm{v}}^{\intercal}, \tag{13}$$

which converts, via an algebraic mapping, the integral relationship expressed in Equation (9). Thus, with Equations (12) and (13), the controller objective function can be expressed now in terms of the coefficient vectors $\hat{\mathrm{f}}_{\mathrm{u}}$, $\hat{\mathrm{f}}_{\mathrm{e}}$, and the force-to-velocity system model G_{o} as

$$J_N = -(\hat{\mathrm{f}}_{\mathrm{e}} - \hat{\mathrm{f}}_{\mathrm{u}})\mathrm{G}_{\mathrm{o}}\frac{T}{2}\hat{\mathrm{f}}_{\mathrm{u}}{}^{\intercal}. \tag{14}$$

Finally, the control optimisation problem for WEC arrays can now be expressed as

$$\begin{aligned} \hat{\mathrm{f}}_{\mathrm{u}}^{\star} \leftarrow & \max_{\hat{\mathrm{f}}_{\mathrm{u}} \in \mathbb{R}^{N}} & & J_N \\ & \text{subject to:} & & \mathcal{C}. \end{aligned} \tag{15}$$

In essence, the optimisation problem described in Equation (15) constitutes a quadratic optimisation problem involving the PTO force $\hat{\mathrm{f}}_{\mathrm{u}}$. Such a problem is subject to a set of constraints $\mathcal{C}$, which stem from the physical limitations inherent to the WEC system. In the specific application discussed in Section 5, the set of constraints $\mathcal{C}$ can be formulated based on parameters such as the maximum device displacement ($X_{\max}$), maximum PTO force ($F_{\max}$), and maximum velocity ($V_{\max}$).

To address the constrained optimisation problem defined in Equation (15), a collocation technique is employed. In this approach, the constraints are enforced at specific time points referred to as collocation points. When considering common constraints like $X_{\max}$ and $F_{\max}$, the set of constraints $\mathcal{C}$ in Equation (10) can be reformulated as a set of linear inequality constraints [53] as shown below:

$$\mathcal{C} := \begin{bmatrix} A_{\mathrm{u}} \\ A_{\mathrm{x}} \end{bmatrix} \hat{\mathrm{f}}_{\mathrm{u}}^{\intercal} \leq \begin{bmatrix} b_{\mathrm{u}} \\ b_{\mathrm{x}} \end{bmatrix}, \tag{16}$$

where

$$\begin{aligned} A_{\mathrm{u}} &= \begin{bmatrix} \Phi(\mathbf{T}_c) \\ -\Phi(\mathbf{T}_c) \end{bmatrix}, \quad A_{\mathrm{x}} = \begin{bmatrix} \Phi(\mathbf{T}_c)\mathrm{G}_{\mathrm{o}} \\ -\Phi(\mathbf{T}_c)\mathrm{G}_{\mathrm{o}} \end{bmatrix}, \\ b_{\mathrm{u}} &= \begin{bmatrix} F_{\max}\hat{\mathbf{1}} \\ F_{\max}\hat{\mathbf{1}} \end{bmatrix}, \quad b_{\mathrm{x}} = \begin{bmatrix} X_{\max}\hat{\mathbf{1}} - \Phi(\mathbf{T}_c)\hat{\mathrm{f}}_{\mathrm{e}} \\ X_{\max}\hat{\mathbf{1}} + \Phi(\mathbf{T}_c)\hat{\mathrm{f}}_{\mathrm{e}} \end{bmatrix}, \end{aligned} \tag{17}$$

where $\hat{\mathbf{1}} \in \mathbb{R}^{2n_{\mathrm{c}}n_{\mathrm{b}} \times 1}$ is a block diagonal matrix of ones with n_{c} the number of chosen collocation points and $\mathbf{T}_c = [t_1, t_2, \ldots t_{n_c}]$ a vector containing the specific time instants at which the constraints are enforced. Leveraging the defined collocation points, general-purpose optimisation solvers, particularly those tailored for quadratic programming (QP), can be applied to address the presented problem.

4. Control Co-Design Algorithm

In this section, the formulation and solution approach for the WEC array CCD problem are introduced. Generally, it is possible to formulate the WEC array CCD scheme as

$$\begin{aligned} \rho^{\mathrm{opt}} \leftarrow & \underset{\rho \in \mathbb{R}^{N}}{\text{Optimise}} & & \Psi \\ & \text{subject to:} \quad \max_{\substack{\hat{\mathrm{f}}_{\mathrm{u}} \in \mathbb{R}^{N} \\ \mathcal{C}}} & & J_N(\rho). \end{aligned} \tag{18}$$

In this case, the optimisation problem aims to minimise or maximise (depending on the definition) the objective function Ψ with respect to the variable ρ, while adhering to the constraints defined by the spectral controller detailed in Equation (15). It should be noted that the structure of the objective function Ψ is contingent upon the unique specifications and needs of the application. In this analysis, the objective function Ψ will encompass the economic evaluation of each array layout ρ, taking into account the optimised control actions for each device in the array.

4.1. CCD objective function definition

As highlighted in Section 1, one of the paramount challenges within wave energy is the substantial reduction of overall expense associated with WEC arrays in order to achieve economic viability. It should be noted that even though this analysis will be primarily centred on WEC arrays, the principles discussed here can also be extrapolated to individual WECs. In the existing literature, the levelised cost of energy (LCoE) stands as the main metric employed to assess the economic viability of diverse energy sources. Thus, the present study introduces an innovative optimisation methodology aiming to determine the optimal configuration for WEC arrays, leveraging a metric derived from LCoE. Traditionally, LCoE (expressed in €/MWh) is articulated as follows:

$$\mathrm{LCoE} = \frac{\mathrm{CapEx} + \mathrm{OpEx}}{\text{Energy production}}, \tag{19}$$

where CapEx and OpEx refer to the capital and operational expenditure of the array, respectively, and the energy production is computed over the projected operational lifespan of the WEC array. To offer a comparative perspective, recent assessments [54] for onshore and fixed-bottom offshore wind energy have suggested LCoE estimates of 38$/MWh and 85$/MWh, respectively.

As mentioned in Section 1, this study exclusively concentrates on the optimisation of WEC array layout, with a homogeneous set of WECs. Hence, the cost variations from one array layout to another

will primarily affect CapEx. Thus, for the purpose of this analysis, OpEx is presumed to be a fraction of CapEx, which ensures that OpEx doesn't exert any influence on the outcome of the optimal array layout. However, it is important to acknowledge that adjustments in the array layout may potentially influence device interaction, impacting WEC behaviour and, subsequently, operation and maintenance needs. Nevertheless, it is reasonable to assume that the costs associated with these effects are relatively negligible compared to CapEx.

The capital expenditure associated with WEC arrays can be further dissected into several components, including the expenses related to site leasing (LeEx), the expenses incurred during device commissioning (ComEx), and the cost of the devices (DevEx) themselves, which can also be subdivided into their individual components. Among such components, the mooring system of the array may exhibit variability depending on the layout under consideration, potentially influencing the cost calculations, since, in certain layouts, two WECs may share specific parts of the mooring system, such as the chain or the anchor. However, since the present study maintains uniform devices across all layouts, most of the components of the WECs are common for all the scenarios and, hence, do not affect the obtained optimal layout. Therefore, for the sake of simplicity, such components of the WECs are excluded from this study. Consequently, the cost of devices in the array can, in this study, be defined as the cost of the mooring system. Note that, when sharing components of the mooring system, such as anchors, the cost savings extend beyond just the anchor itself. This includes the cost associated with its installation, which can be categorised as part of the commissioning cost (ComEx). In practice, considering that the cost of the anchor for a catenary mooring is proportionate to the horizontal force, sharing an anchor could, depending on the array layout, effectively lower its cost, since the layout can be designed so that the forces exerted by the two moorings mitigate each other, resulting in reduced anchor costs.

Finally, the sole commissioning expense taken into account pertains to the installation of the mooring anchor, since it is the only cost that fluctuates depending on the layout. Other commissioning expenses are presumed to remain constant irrespective of the layout under consideration and, hence, will not affect the obtained outcome of the analysis. Thus, it is possible to define a new performance function, similar to that in Equation (19), as

$$\mathrm{LCoE}^* = \frac{\mathrm{CapEx}^*}{E}, \tag{20}$$

with the generated energy E as in Equation (9), and CapEx^* containing all the costs derived from the mooring system of the array (mooring lines and anchors), as well as the site leasing cost (which depends on the layout size).

4.2. CCD problem solution

The problem described in Equation (18) is typically addressed, as documented in [34], through one of the following approaches:

- **Control-inspired** approaches draw upon engineering expertise in dynamics and control principles. They propose novel control solutions based on simplified models and control engineering techniques.
- **Co-optimisation** techniques employ mathematical methodologies that incorporate nonlinear models and optimisation theory. It considers the cost function associated with the plant architecture, dynamics, and controller design. It allows for modifications to the system structures throughout the optimisation process.
- **Co-simulation** methods utilise dynamic models of varying fidelity in iterative simulations. They integrate optimisation algorithms, data-driven models, and machine learning techniques. Co-simulation proves advantageous in managing the complexity of CCD problems, enabling the integration of models, iterative refinement of designs, and flexibility in exploring different design options.

In summary, co-simulation emerges as a potent methodology for discovering optimal solutions within the realm of CCD problems [34]. It facilitates a thorough analysis of system dynamics, streamlines the exploration of design alternatives, and shortens the design cycle. Co-simulation can seamlessly integrate models spanning multiple scales and physics domains, encompass optimisation algorithms and data-driven methodologies, and offer a modular approach to design. The interested reader is referred to [34] for more in-depth insights into CCD solution strategies.

In this study, a co-simulation approach is adopted to address the CCD problem outlined in Equation

(18). Ideally, this co-simulation method could be coupled with an optimal point search algorithm, such as linear or binary search techniques. However, for the sake of giving informative results for all potential array layouts, an exhaustive search procedure is considered here. This parametric study entails computing outcomes for every conceivable WEC array layout, ultimately revealing which configuration minimises the objective function described in Section 4.1, but also showing sensitivity to parameter variation. The advantage of this approach lies in its ability to furnish a comprehensive overview of the search space.

5. Case Study

In this section, an illustrative example is presented to emphasise the advantages of the CCD method introduced in this paper. This methodology is applied to a specific case study to demonstrate the benefits and potential enhancements that can be achieved by integrating advanced control strategies with system design, rather than relying on simple passive controllers. Through this example, the significance of incorporating control considerations from the early stages of system development is highlighted, leading to improved performance and optimised outcomes in practical applications.

5.1. Realistic Climate

In this analysis, a comprehensive evaluation of the energy generated by the WEC array at a specific location is pursued. Thus, as mentioned in Section 4.1, the consideration of various sea states to assess the performance of a WEC array on a specific site is necessary, with these sea states being selected based on the probability distribution of their occurrence at the designated site, a representation commonly depicted using a scatter diagram [55]. It is important to note that while calculating energy production, a 20-year operational lifespan is assumed for the array but, for simplicity, no potential variations in sea state intensity over time are accounted for here (such as the potential increase in intensity and aggressiveness of sea states as time progresses, as illustrated in [56]).

For this study, the chosen location is BIMEP, an offshore test site located in the Bay of Biscay off the Basque coast [57]. In order to include the information of the site within the considered CCD problem, it is necessary to characterise the wave conditions of the given site with a finite number of sea states. To this end, the 16 most relevant sea states (from an electricity generation perspective [57]) have been chosen in this analysis, as shown in Figure 1.

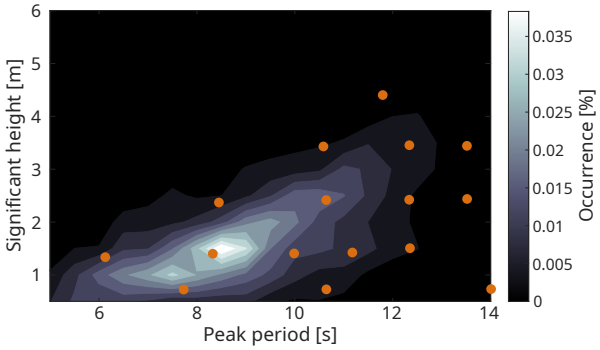

Figure 1: Scatter diagram of the wave conditions at BIMEP with the chosen sea states denoted with orange dots [57].

In addition to accounting for the most significant sea states, it is imperative to take into consideration the various potential wave directions at a site to ensure the optimal layout of the array. In this particular scenario, as depicted in Figure 2, it is evident that waves primarily approach BIMEP from a single direction. Therefore, for the CCD problem at hand, a single wave direction is considered.

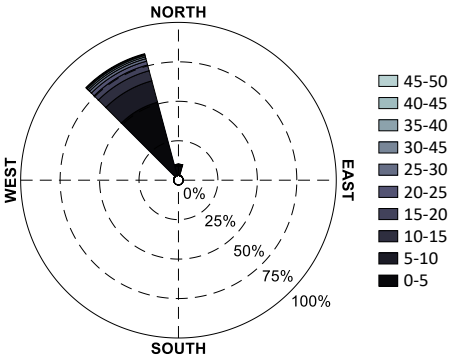

Figure 2: Wind rose at BIMEP.

Finally, in order to be statistically consistent, the results for each of the chosen sea states are derived by averaging the outcomes across several realisations (10 in this instance) of each sea state. Then, it is assumed that the acquired results are applicable for a specific number of days within the 20-year operational lifespan, depending on the frequency of occurrence of each sea state, as shown in Figure 1.

5.2. WEC device and array

The WEC array considered here comprises five identical heaving point absorbers aligned in a linear array configuration. It should be noted that assuming the WECs exclusively exhibit heave motion represents a significant simplification since the optimisation algorithm incorporates the mooring system into the objective function, and takes into account that additional DoFs would considerably affect the mooring configuration selection. Furthermore, accounting for surge and sway motion would require careful consideration of the minimum inter-device distance to prevent collisions. However, for the purpose of this study, which aims to demonstrate the proposed methodology in a straightforward manner, the simplifying assumption that the WECs move solely in heave is retained.

The device selected for this analysis is inspired by the MARMOK-A-5 WEC illustrated in Figure 3, which is a spar-like floating oscillating water column (OWC) [58, 59] developed by IDOM. Among the different wave energy converter prototypes, OWC devices seem to be one of the most promising technologies [60], being a robust and reliable solution to extract the untapped energy from ocean waves. In addition, the MARMOK-A-5 was deployed at the BIMEP test site for over two and a half years using a mooring configuration similar to the one suggested here (see Section 5.3).

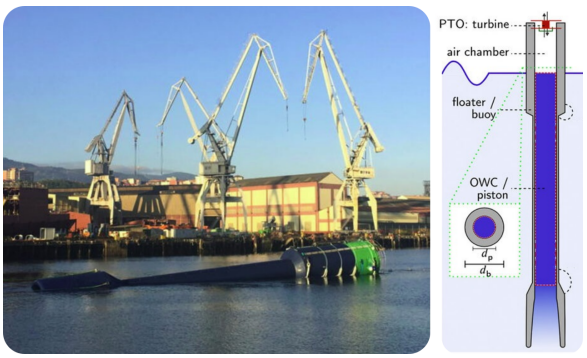

Figure 3: Illustration of the floating OWC device MARMOK-A-5 developed by IDOM [61].

However, due to the complexity associated with modelling an OWC concept, the device is simplified as a single-body cylindrical point absorber with the same geometric characteristics as the MARMOK-A-5 floater. Due to the geometric similarities, the hydrodynamic behaviour of the simplified device is expected to be similar to the MARMOK-A-5 WEC and, thus, conclusions extracted from the present study can be considered valid.

Furthermore, an increasing interest in arrays of similar devices can be found within the wave energy literature, *e.g.* [30] analysing different mooring configurations for similar devices in arrays of 5 devices and [27] using the same geometry approximation for assessing the performance of arrays of different sizes. In the current study, the array layout consists of 5 devices in line, as illustrated in Figure 4. The decision is based on different studies in the literature as, for example, [40] where a similar array layout that uses the KARRATU mooring configuration is suggested. Furthermore, [27] concludes that small arrays of up to 5 devices are hydrodynamically more effective. In fact, [30] also suggests an array of 5 devices.

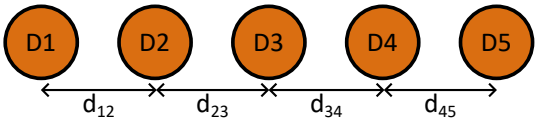

Figure 4: WEC array layout considered in this study.

As mentioned before, the primary objective of this study is to demonstrate the applicability of the proposed CCD scheme for optimising array layouts. To achieve this, various inter-device distances and array alignments are considered for the layout depicted in Figure 4. However, it should be noted that, in order to simplify the representation of the results (and reduce the number of cases), it is assumed that the array under study is symmetric for all the cases analysed, i.e. $\mathbf{d_{12}}$=$\mathbf{d_{45}}$ and $\mathbf{d_{23}}$=$\mathbf{d_{34}}$. Thus, a set of 19 different inter-device distances (ranging from 2 to 20⌀) are considered here for $\mathbf{d_{12}}$ and $\mathbf{d_{23}}$. Additionally, three different alignments of the array with respect to the incoming waves which, as mentioned in Section 5.1, are considered to have a single wave direction are analysed. In particular, the three considered alignments are 0° (array perpendicular to wave direction, the wave front arrives at all the WECs at the same time), 45° (intermediate case), and 90° (in line with the wave direction, incoming waves travel from D1 to D5, see Figure 4). Thus, the aforementioned inter-device distances and array alignments are assessed to determine the optimal array configuration for the BIMEP location.

5.3. Mooring Configurations: KARRATU

Several mooring configurations have been presented in the literature, paving the way towards the development of innovative solutions for the station keeping of ORE devices. The purpose of these innovations is to either reduce the cost of the mooring systems or enhance their performance, including offset reduction and peak load mitigation. Such innovative configurations range from simple chain catenaries anchored to the seabed to mixed material mooring lines connected by floating elements, clump weights, and novel elastomeric tethers [62].

Among the different solutions, KARRATU has been presented in the literature as a compliant modular mooring configuration. As shown in Figure 5, it is composed of a square design of wires, whose corners are connected to fairleads of the device via polyester lines. At each corner, a floating surface buoy is located and connected to the seabed through a catenary chain. In [40], the KARRATU concept is introduced for an array of floating point absorbers. The main advantage of the KARRATU is the reduction of impedance and damping related to the mooring system while increasing the freedom of device movement. This concept has been successfully installed and tested for a single MARMOK-A-5 device during the EU-funded OPERA project [63].

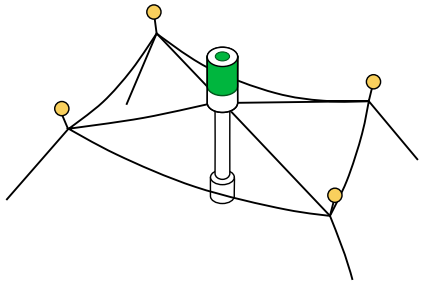

Figure 5: Sketch of the KARRATU mooring configuration, adapted from [64].

5.4. LCoE* calculation

As introduced in Section 3.1, the only costs considered for the CCD problem are those that vary with the array layout: i.e. mooring and leasing costs. Thus, the costs associated with the KARRATU mooring system can be divided into the individual costs of different components: Anchors, catenary legs, surface buoys, umbilical cable, cables connecting the four surface buoys[1], and the cables connecting the buoys with the WEC. It should be noted that the cost of the intra-array cables is not considered here, since it would depend on the selected connection configuration (in series or in parallel) and the location of the substation. Similarly, the cost of the dynamic cables connecting the devices to the static ones has not been included as it does not depend on the layout. Additionally, the cost of the surface buoys is also not considered, since it is negligible compared to the cost of the other components [65].

The array mooring configuration (and, hence, its cost) depends on the inter-device distances associated with each specific layout. Thus, as shown in Figure 6, for any WEC pair, three different configurations are considered:

- If the inter-device distance between bodies i and j (d_{ij}) is larger than d_{an} (i.e. the distance between two subsequent anchors of the same WEC), the devices are moored in a separate fashion and, hence, each WEC has two independent mooring systems (see Figure 6.a). In this case, the cost of the mooring for the two devices is given by:

$$\text{MooEx}^* = 2\left(4c_{an} + 4c_{ch}L_{ch} + 4c_{ss}L_{ss}\right), \quad (21)$$

  where c_{an} is the cost of each anchor, c_{ch} the cost per unit length of the chain used for the mooring legs, L_{ch} the length of such chains, c_{ss} the cost per unit length of the elastic fibre used for the square sides, and $L_{ss} = 2\varnothing$ the length of each side.

- If $2\varnothing < d_{ij} \leq d_{an}$, as shown in Figure 6.b, the two WECs share two of the anchors but, apart from that, have their own separate mooring system. For this case, the cost of the mooring is defined as

$$\text{MooEx}^* = 6c_{an} + 8c_{ch}L_{ch} + 8c_{ss}L_{ss}. \quad (22)$$

- Finally, if the inter-device distance is $2\varnothing$, the KARRATU systems of the two devices are connected, sharing one of the square connectors side, two of the anchors and two of the mooring legs (as illustrated in Figure 6.c). The mooring cost for this case is expressed as

$$\text{MooEx}^* = 6c_{an} + 6c_{ch}L_{ch} + 7c_{ss}L_{ss}. \quad (23)$$

[1] Note that the cost of such cables is not considered here, since it does not vary with the layout configuration.

Note that, for the sake of simplicity, in this study, the previous configurations and mooring costs (as given in Equations (21)-(23)) are presented for a single pair of devices. However, in this analysis, five WECs are considered. Consequently, the total cost of the mooring systems of all five devices, for each given layout, is computed by combining the introduced three mooring configurations. Note that the choice of the mooring configurations for each layout depends on the specific inter-device distances of the layout being analysed.

The costs of the anchors (c_{an}), chain (c_{ch}), and elastic fiber (c_{ss}) are obtained from [65], and are presented in Table 1. It should be noted that, owing to the scarcity of accessible information on mooring costs for WECs, the costs outlined in [65] are incorporated here, despite that the primary focus of [65] is on floating offshore wind platforms. Regarding installation costs, those introduced in [65] are considered here, i.e c_{in} = 44k€/anchor.

Table 1: Cost of the mooring components from [65].

Material	Cost
Anchor	114k €/anchor
Chain	755 €/m
Elastic fibre	182 €/m

Finally, the leasing cost of the deployment site is determined based on the approach described in [66], with the assumption that it constitutes roughly one-third of the total mooring system cost. Consequently, when considering an independent device with its own mooring system, the leasing cost per linear meter can be computed as follows:

$$c_{le} = \frac{4c_{an} + 4c_{ch}L_{ch} + 4c_{ss}L_{ss} + 4c_{in}}{3d_{an}}. \quad (24)$$

In this case, the leasing cost per linear meter of the deployment site is $c_{le} \approx 11.7$k€/m and, to obtain the total cost, must be multiplied by the total length of the array (L_{ar}, as shown in Figure 6). Thus, the LCoE* from Equation (20) can be now expressed for the specific case as

$$\text{LCoE}^* = \frac{\text{MooEx}^* + L_{ar}c_{le}}{E}, \quad (25)$$

with the absorbed energy E calculated over the 20 years of operational lifespan, as introduced in Section 5.1. The sum of all the considered costs is shown in Figure 7 for all the array layouts analysed here. Since the layout is symmetric, the costs

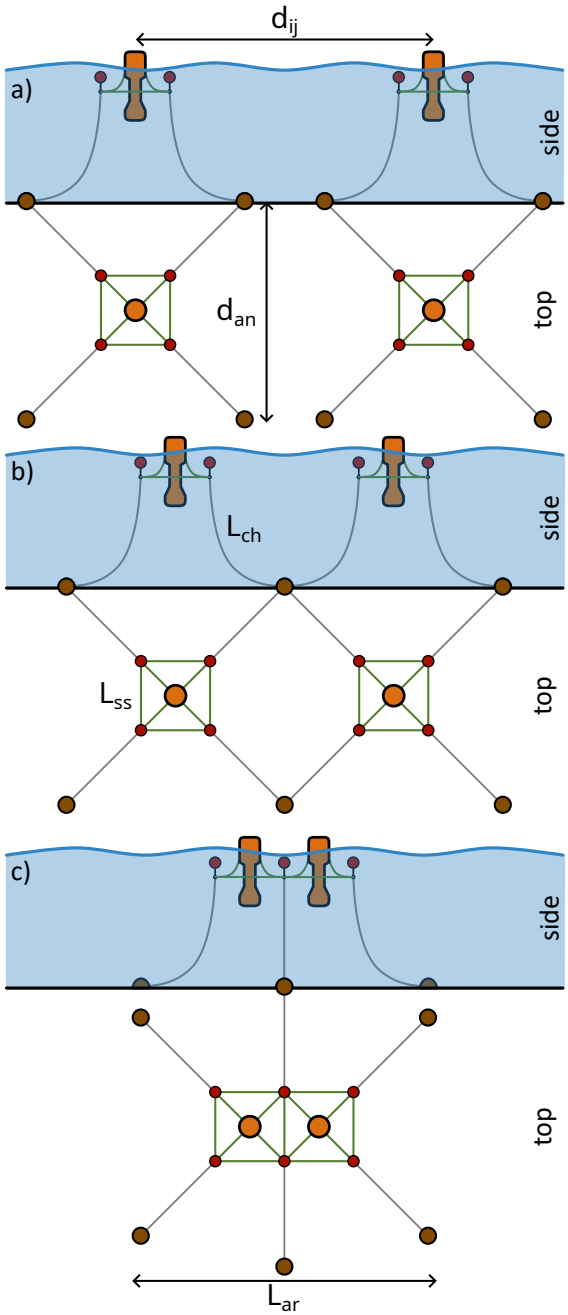

Figure 6: Sketch of the different mooring configurations depending on the inter-device distance.

(and the results in general) can be shown as a function of d_{12} and d_{23}. The jumps in the cost result from changing from one mooring configuration to another one with more sub-components, with the lowest cost at d_{12}=d_{23}=2⌀, where the five devices are connected through their KARRATU systems

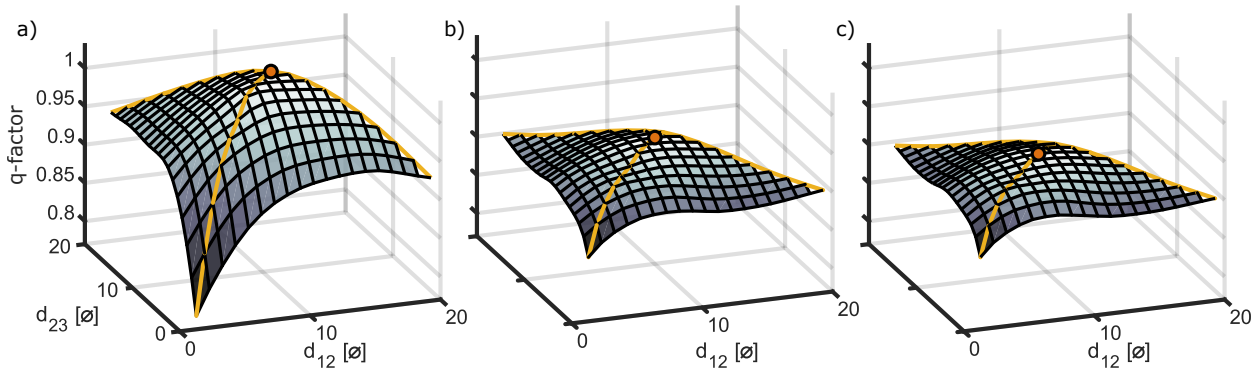

Figure 8: q-factor obtained from the energy absorbed during the 20 years of lifespan for all the array layouts considered, with different array alignments with respect to the incoming wave: (a) 0°, (b) 45°, and (c) 90°. The orange dot represents the maximum value. The yellow lines in (a), (b), and (c) delineate the cross-sections for the analyses depicted in Figure 9. Specifically, the equidistant cross-section, where $d_{12} = d_{23}$, is represented by a yellow dashed line, while the maximum distance cross-section, where $d_{12} + d_{23} = 22\varnothing$, is depicted by a solid yellow line.

(see Figure 6.c). Note that the first step in Figure 7, at $8\varnothing$, is due to locating the mooring anchor at $6\varnothing$ from the device. Thus, $8\varnothing$ represents the inter-device distance beyond which two (four, due to symmetry) devices are too distant from each other to share a common anchor (as depicted in Figure 6.b). Furthermore, the highest is in Figure 7 referring to the scenario where the five devices have independent mooring systems (Figure 6.a). Finally, the increasing slope of the cost is given by the leasing cost of the site.

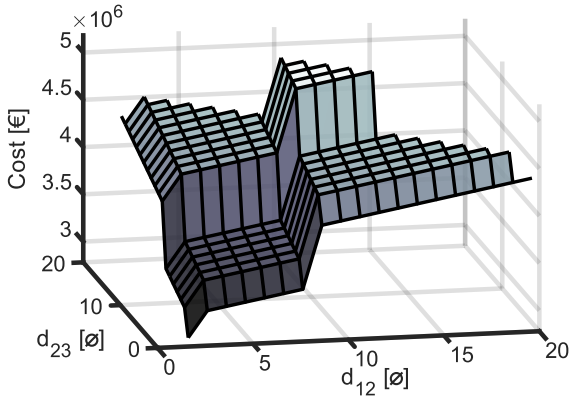

Figure 7: Considered costs for all the array layouts under study.

6. Results & discussion

This section presents and discusses the outcomes derived from the application of the presented CCD methodology for mooring layout design. It is important to note that the results are notably influenced by the costs outlined in the previous section, which may not perfectly align with the actual costs specific to this problem. Consequently, the results presented here should not be interpreted as the definitive optimal array layout for BIMEP, but rather as an illustrative study demonstrating the importance of employing CCD approaches for optimizing WEC arrays.

To present the results more clearly, the absorbed energy is expressed by means of the q-factor, as initially introduced in Section 1 (see Equation (1)). In this light, it should be noted that the energy absorbed by an isolated device during the 20 years of operation is 580 MWh. Thus, Figure 8 shows the q-factor obtained by the different array layouts and alignments considered.

One could notice that the highest q-factor is obtained for the array aligned perpendicularly to the wave direction, i.e. the 0° case illustrated Figure 8.a, for an inter-device distance of d_{12}=d_{23}=$11\varnothing$ (with a total absorbed power of 2.97 GWh. However, the case shown in Figure 8.a is also the most varying one among the three, with the minimum absorbed energy at the array configuration with the closest distance, i.e. d_{12}=d_{23}=$2\varnothing$, due to the destructive interactions. On the contrary, the other two analysed array alignments obtain a less varying but lower energy absorption, with their maximums at 2.71 GWh and 2.70 GWh for Figures 8.b and 8.c, respectively. Interestingly, despite the fact that the results are not symmetric, all the maximums happen on an array layout with equidistant inter-device distances.

For further details on the absorbed energy, Figure

9 shows, all together, the q-factor obtained with the equidistant layouts (Figure 9.a), i.e. $d_{12} = d_{23}$, and the layouts with the maximum inter-device distance (Figure 9.b), i.e. the distance from D1 to D5 which, in this case, is 44⌀. Note that, for clarity, such two specific cases are also highlighted in Figure 8.

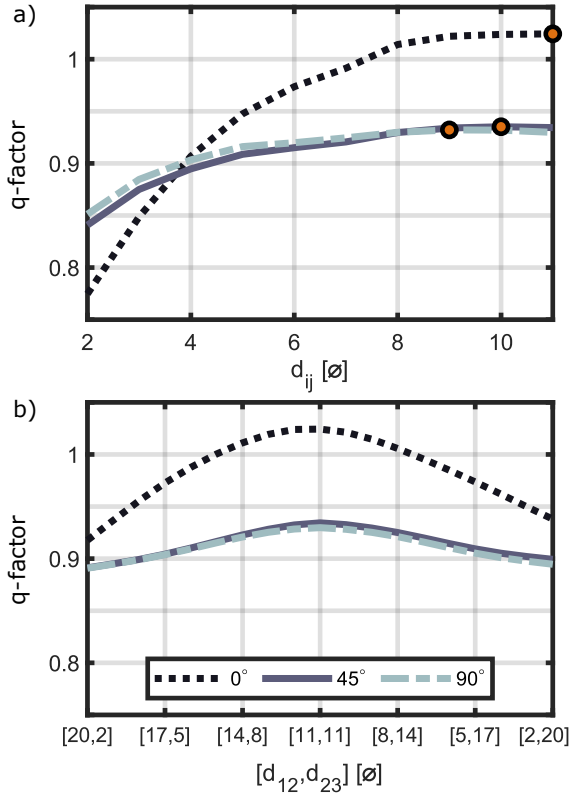

Figure 9: Cross-section analyses of the absorbed energy. In (a) the equidistant cross-section analysis, represented by a yellow dashed line in Figure. 8, and in (b) the maximum inter-device distance cross-section analysis, depicted with a solid yellow line in Figure. 8.

Figure 9.a shows that, due to more destructive interactions, the layouts aligned at 0° generate less energy than those aligned at 45° and 90° for inter-device distances of less than (approximately) 4⌀, despite being the case obtaining the highest energy absorption (at d_{12}=d_{23}=11⌀). One could notice that no strong effect of the interactions can be appreciated on the absorbed energy shown in Figure 9.a. This is because, depending on the peak period of the sea state, the main interaction effects appear at different inter-device distances and, by considering a large variety of sea-states as in this study, such interaction effects are attenuated. However, it is important to emphasise that, with a sufficiently large inter-device distance, the q-factor shown in Figure 9.a should converge to 1, representing isolated device cases.

Furthermore, Figure 9.b shows that the energy absorbed by the layouts is not symmetric with respect to the equidistant inter-device-distance-axis. In particular, such an asymmetry can be easily appreciated for the 0° layouts, where the cases with larger d_{23} (compared to d_{12}) obtain higher energy absorption (and, hence, q-factor). Thus, the layouts with two pairs of WECs in the corners and the separated device in the middle obtain more energy than the layouts with three devices next to each other in the middle and two separate devices in the corners.

Finally, Figure 10 shows the LCoE* values (see Equation (25)) obtained for all the layouts considered. One key aspect to highlight is that the results shown in Figure 10 closely mirror (inverted, due to the inversion of the z axis) the structure of the costs illustrated in Figure 7. This is because the absorbed energy does not have much variation (compared to the cost) and, hence, when dividing the costs by the energy (see Equation (25)), it retains the shape of the former. Consequently, the optimal case (from an economical perspective) for the arrays aligned at 45° and 90° (Figures 10.b and Figure 10.c, respectively) is the case with the lowest costs (despite the fact that is also the case with the lowest energy production), i.e. d_{12}=d_{23}=2⌀. Conversely, for the arrays aligned at 0°, the optimal LCoE* is not obtained at the lowest cost case since, as shown in Figure 8.a, the differences between lowest and highest energy absorption cases in this scenario are larger, counteracting the low cost of the closest inter-device distances. In particular, in Figure 10.a the optimal case happens at d_{12}=2⌀ and d_{23}=8⌀ which: (i) on the one hand, is on the limit to not have any device with an independent mooring system which, as explained for Figure 7, highly increases the cost; and (ii) on the other hand, it represents, from the asymmetric layouts, the distribution with higher energy absorption (two device pairs on the corners and a WEC separated in the middle, i.e. D2 and D3 closer to D1 and D5 than to D3), as explained before for Figure 9.b.

The optimal LCoE* values in Figure 10 are 0.119 €/kWh, 0.114 €/kWh, and 0.113 €/kWh for the 0°, 45°, and 90° alignments, respectively. Hence, in the present study, the obtained optimal array for the considered location (BIMEP) should

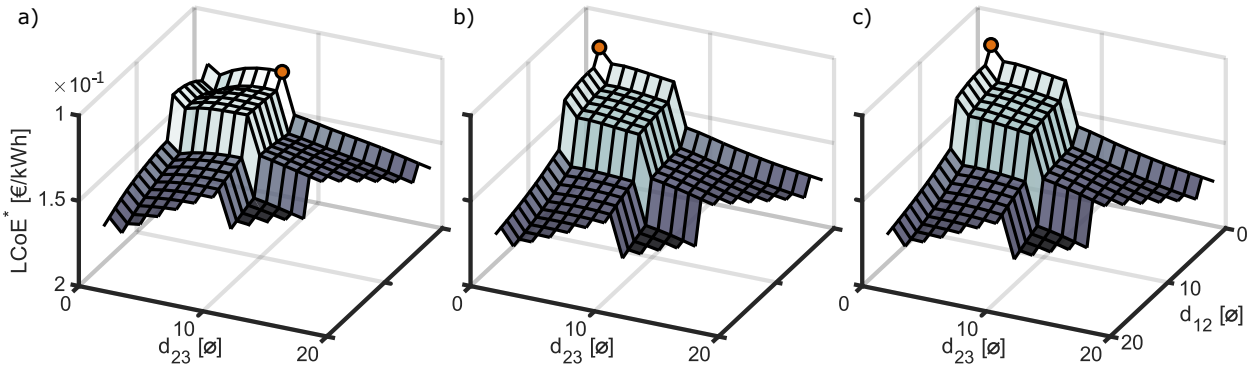

Figure 10: LCoE* values (obtained as in Equation (25)) for all the layouts considered, with different alignments between the array and incoming wave: (a) 0°, (b) 45°, and (c) 90°. Note that the z-axis is inverted to improve the visualisation of the results, and the minimum value is highlighted in orange.

be located in line with respect to the wave direction and with an inter-device distance of d_{12}=d_{23}=2⌀. As mentioned at the beginning of the section, the obtained result does not necessarily mean that such an array is optimal for BIMEP in reality since that is not the aim of the present case study but rather to show how, with the considered CCD approach, it is possible to assess the optimal array layout from an economic perspective, considering the presence of an advanced control strategy. In fact, considering that the obtained LCoE* values only account for the mooring systems (and are already significantly high), it is possible to assume that a different[2] mooring system should probably be considered in this case study, in order to reduce costs, which would change the obtained results.

7. Conclusion

The current study proposes a CCD methodology for array layout design from an economic perspective, with an application case aimed at demonstrating the effectiveness of such CCD algorithm in a realistic context. To this end, the current study considers (i) 20 years of actual sea states (and their historical probabilities) at the BIMEP test site to compute the WEC array energy production, (ii) a realistic WEC (MARMOK-A-5-like device) that was deployed at such test site for two years, and (iii) a mooring configuration (termed KARRATU) that was developed for such device. Additionally, the study meticulously includes the mooring costs by separately analysing all the components of the KARRATU system, deriving the costs using insights from offshore floating wind literature.

The results provide clear insights into the energy absorption by the different array layouts considered (changing the inter-device distances and alignments with respect to the incoming waves). The highest energy absorption is observed when the array is aligned perpendicularly to the wave direction, with an equidistant inter-device distance of $d_{12} = d_{23} = 11⌀$. However, the study suggests that the optimal array layout, from an economical perspective, should align with the wave direction and maintain an inter-device distance of $d_{12} = d_{23} = 2⌀$.

This study underscores the critical importance of adopting a CCD approach to assess optimal array layouts from an economic perspective while integrating advanced control strategies. It highlights a significant observation - the optimal layout for economic factors might not align with the optimal choice based solely on technical factors, such as energy absorption, as demonstrated in the presented case study. In fact, for the study at hand, it was counterintuitive that one of the most economically favourable layouts was among the least energy-efficient. While these specific findings may not prescribe the ideal BIMEP array layout in practice, they strongly underscore the necessity of employing a CCD approach, as presented in this study, when designing wave energy converter arrays. This approach ensures that array designs consider not only energy absorption but also economic considerations, contributing to a more comprehensive and

[2]Note that, as introduced in Section 5.3, the costs of the considered mooring systems come from an offshore floating wind study, due to the lack of information on this matter for WECs.

balanced decision-making process.

Acknowledgment

The authors at Mondragon University are funded by the research project PID2021-124245OA-I00 funded by MCIN/AEI/10.13039/501100011033 and by ERDF A way of making Europe, and the research project funded by the Basque Government's ELKARTEK 2022 program under the grant No. KK-2022/00090. In addition, Yerai Peña-Sanchez is funded by the European Union's Horizon 2020 research and innovation programme under the Marie Sklodowska-Curie grant agreement N°10103429, Demián García-Violini is supported by the Agencia I+D+i from the Government of Argentina under grant PICT-2021-I-INVI-00190, and John Ringwood is supported by Science Foundation Ireland (SFI) through the MaREI Centre for Energy, Climate and Marine under Grant No. 12/RC/2302_P2. Vincenzo Nava's work is funded by the Spanish Ministry of Science and Innovation projects with references TED2021-132783B-I00,PID2019-108111RB-I00 MCIN/AEI/10.13039/501100011033; the Spanish Ministry of Economic Affairs and Digital Transformation project with reference MIA.2021.M04.0008; the "BCAM Severo Ochoa" accreditation of excellence CEX2021-001142-S/MICIN / AEI/10.13039/501100011033; and the Basque Government, Spain through the BERC 2022–2025 program.

References

[1] UN, Adoption of the paris agreement (2015).
URL https://www.iea.org/publications/freepublications/publication/ElectricityInformation2017Overview.pdf

[2] IPCC, SYNTHESIS REPORT OF THE IPCC SIXTH ASSESSMENT REPORT (AR6), Tech. Rep. ISBN 978-92-9169-151-7, Intergovernmental Panel on Climate Change (IPCC) (2023).
URL https://report.ipcc.ch/ar6syr/pdf/IPCC_AR6_SYR_SPM.pdf

[3] IPCC, Global Warming of 1.5oC, Tech. Rep. ISBN 978-92-9169-151-7, Intergovernmental Panel on Climate Change (IPCC) (2018).

[4] IRENA, Future of Wind: Deployment, investment, grid integration and socio-economic aspects (A Global Energy Transformation paper), Tech. Rep. ISBN: 978-92-9260-121-8, International Renewable Energy Agency, Abu Dhabi, available in https://www.irena.org/publications/2019/Apr/Global-energy-transformation-A-roadmap-to-2050-2019Edition (Apr. 2019).

[5] Stéphanie Bouckaert, A. F. Pales, C. McGlade, U. Remme, B. Wanner, Net Zero by 2050: A Roadmap for the Global Energy Sector, Tech. rep., International Energy Agency, Paris (2021).
URL https://www.iea.org/reports/net-zero-by-2050

[6] Ocean Energy Europe, 2030 Ocean Energy Vision, Tech. rep. (2020).
URL https://www.oceanenergy-europe.eu/wp-content/uploads/2020/10/OEE_2030_Ocean_Energy_Vision.pdf

[7] NREL, Marine Energy in the United States : An Overview of Opportunities, Tech. Rep. February (2021).
URL https://www.nrel.gov/docs/fy21osti/78773.pdf

[8] B. Guo, J. V. Ringwood, A review of wave energy technology from a research and commercial perspective, IET Renewable Power Generation 15 (14) (2021) 3065–3090. doi:10.1049/rpg2.12302.

[9] K. Wang, Z. Wang, S. Sheng, Y. Zhang, Z. Wang, Y. Ye, W. Wang, H. Lin, Z. Huang, A method for large-scale wec connecting to island isolated microgrid based on multiple small power hpgss, Renewable Energy (2023) 119330.

[10] F. Fusco, G. Nolan, J. V. Ringwood, Variability reduction through optimal combination of wind/wave resources–an irish case study, Energy 35 (1) (2010) 314–325.

[11] S. Astariz, G. Iglesias, Output power smoothing and reduced downtime period by combined wind and wave energy farms, Energy 97 (2016) 69–81.

[12] W. Sasaki, Predictability of global offshore wind and wave power, International journal of marine energy 17 (2017) 98–109.

[13] A. Pecher, J. P. Kofoed, Handbook of ocean wave energy, Springer Nature, 2017.

[14] IRENA, OEE, Scaling up investments in ocean energy technologies, Tech. rep., International Renewable Energy Agency, Abu Dhabi (2023).

[15] F. Teixeira-duarte, D. Clemente, G. Giannini, P. Rosa-santos, F. Taveira-pinto, Review on layout optimization strategies of offshore parks for wave energy converters, Renewable and Sustainable Energy Reviews 163 (May) (2022) 112513. doi:10.1016/j.rser.2022.112513.
URL https://doi.org/10.1016/j.rser.2022.112513

[16] P. B. Garcia-Rosa, G. Bacelli, J. V. Ringwood, Control-informed optimal array layout for wave farms, IEEE Transactions on Sustainable Energy 6 (2) (2015) 575–582. doi:10.1109/TSTE.2015.2394750.

[17] G. Thomas, D. Evans, Arrays of three-dimensional wave-energy absorbers, Journal of Fluid Mechanics 108 (1981) 67–88.

[18] M. Simon, Multiple scattering in arrays of axisymmetric wave-energy devices. part 1. a matrix method using a plane-wave approximation, Journal of Fluid Mechanics 120 (1982) 1–25.

[19] M. Göteman, M. Giassi, J. Engström, J. Isberg, Advances and challenges in wave energy park optimization—a review, Frontiers in Energy Research 8 (2020) 26.

[20] M. Göteman, J. Engström, M. Eriksson, J. Isberg, Optimizing wave energy parks with over 1000 interacting point-absorbers using an approximate analytical method, International Journal of Marine Energy 10

(2015) 113–126.
[21] B. Child, V. Venugopal, Optimal configurations of wave energy device arrays, Ocean Engineering 37 (16) (2010) 1402–1417.
[22] M. Penalba, T. Kelly, J. Ringwood, Using nemoh for modelling wave energy converters: A comparative study with wamit, in: 12th European Wave and Tidal Energy Conference (EWTEC), 2017.
[23] WAMIT, Wamit, https://www.wamit.com, online accessed 1-Jun-2023 (2023).
[24] A. Babarit, Impact of long separating distances on the energy production of two interacting wave energy converters, Ocean Engineering 37 (8-9) (2010) 718–729.
[25] A. De Andrés, R. Guanche, L. Meneses, C. Vidal, I. Losada, Factors that influence array layout on wave energy farms, Ocean Engineering 82 (2014) 32–41.
[26] S. Bozzi, M. Giassi, A. M. Miquel, A. Antonini, F. Bizzozero, G. Gruosso, R. Archetti, G. Passoni, Wave energy farm design in real wave climates: the italian offshore, Energy 122 (2017) 378–389.
[27] A numerical study on the hydrodynamic impact of device slenderness and array size in wave energy farms in realistic wave climates, Ocean Engineering 142 (2017). doi:10.1016/j.oceaneng.2017.06.047.
[28] P. Lamont-Kane, M. Folley, T. Whittaker, Investigating uncertainties in physical testing of wave energy converter arrays, in: Proceedings of the 10th European Wave and Tidal Energy Conference (EWTEC 2013), Aalborg, Denmark, 2013, pp. 2–5.
[29] V. Stratigaki, P. Troch, T. Stallard, D. Forehand, J. P. Kofoed, M. Folley, M. Benoit, A. Babarit, J. Kirkegaard, Wave basin experiments with large wave energy converter arrays to study interactions between the converters and effects on other users in the sea and the coastal area, Energies 7 (2) (2014) 701–734.
[30] B. Howey, K. M. Collins, M. Hann, G. Iglesias, R. P. Gomes, J. C. Henriques, L. M. Gato, D. Greaves, Compact floating wave energy converter arrays: Inter-device mooring connectivity and performance, Applied Ocean Research 115 (2021) 102820.
[31] T. Vervaet, V. Stratigaki, B. De Backer, K. Stockman, M. Vantorre, P. Troch, Experimental modelling of point-absorber wave energy converter arrays: A comprehensive review, identification of research gaps and design of the wecfarm setup, Journal of Marine Science and Engineering 10 (8) (2022) 1062.
[32] N. Faedo, Y. Peña-Sanchez, E. Pasta, G. Papini, F. D. Mosquera, F. Ferri, Swell: An open-access experimental dataset for arrays of wave energy conversion systems, Renewable Energy 212 (2023) 699–716.
[33] A. Mérigaud, J. V. Ringwood, Improving the computational performance of nonlinear pseudospectral control of wave energy converters, IEEE Transactions on Sustainable Energy 9 (3) (2018) 1419–1426. doi:10.1109/TSTE.2017.2786045.
[34] M. Garcia-Sanz, Control co-design: An engineering game changer, Advanced Control for Applications: Engineering and Industrial Systems 1 (1) (2019) e18.
[35] R. G. Coe, G. Bacelli, S. Olson, V. S. Neary, M. B. R. Topper, Initial conceptual demonstration of control co-design for WEC optimization, Journal of Ocean Engineering and Marine Energy 6 (4) (2020) 441–449. doi:10.1007/s40722-020-00181-9.
[36] Y. Peña-Sanchez, D. García-Violini, J. V. Ringwood, Control co-design of power take-off parameters for wave energy systems, IFAC-PapersOnLine 55 (27) (2022) 311–316. doi:https://doi.org/10.1016/j.ifacol.2022.10.531.
[37] C. Fitzgerald, G. Thomas, A preliminary study on the optimal formation of an array of wave power devices, in: Proceedings of the 7th European Wave and Tidal Energy Conference, Porto, Portugal, 2007, pp. 11–14.
[38] H. Wolgamot, P. Taylor, R. E. Taylor, The interaction factor and directionality in wave energy arrays, Ocean Engineering 47 (2012) 65–73.
[39] M. Göteman, J. Engström, M. Eriksson, J. Isberg, M. Leijon, Methods of reducing power fluctuations in wave energy parks, Journal of Renewable and Sustainable Energy 6 (4) (2014).
[40] P. Ricci, A. Rico, F. Boscolo, J. L. Villate, Design , Modelling and Analysis of an Integrated Mooring System for Wave Energy Arrays, in: 4th International Conference on Ocean Energy, Dublin, Ireland, 2012.
[41] X. Shao, J. W. Ringsberg, H.-D. Yao, Z. Li, E. Johnson, G. Fredriksson, A comparison of two wave energy converters' power performance and mooring fatigue characteristics–one wec vs many wecs in a wave park with interaction effects, Journal of Ocean Engineering and Science (2023).
[42] J. B. Thomsen, F. Ferri, J. P. Kofoed, K. Black, Cost optimization of mooring solutions for large floating wave energy converters, Energies 11 (1) (2018) 159.
[43] Y. Peña-Sanchez, D. García-Violini, A. Zarketa, M. Penalba, V. Nava, J. V. Ringwood, Wave energy converter array layout control co-design for different mooring configurations, in: 15th European Wave and Tidal Energy Conference, no. September, Bilbao, Spain, 2023, p. 531. doi:10.36688/ewtec-2023-531.
URL https://doi.org/10.36688/ewtec-2023-531
[44] T. F. Ogilvie, Recent progress toward the understanding and prediction of ship motions, in: 5th Symposium on Naval Hydrodynamics, Vol. 1, Bergen, Norway, 1964, pp. 2–5.
[45] J. Falnes, Ocean Waves and Oscillating Systems: Linear Interactions Including Wave-Energy Extraction, Cambridge Univ. Press, 2002.
[46] D. García-Violini, Y. Peña-Sanchez, N. Faedo, J. V. Ringwood, An energy-maximising linear time invariant controller (LiTe-Con) for wave energy devices, IEEE Transactions on Sustainable Energy 11 (4) (2020) 2713–2721.
[47] H. Kagemoto, D. K. Yue, Interactions among multiple three-dimensional bodies in water waves: an exact algebraic method, Journal of Fluid mechanics 166 (1986) 189–209.
[48] J. C. McNatt, V. Venugopal, D. Forehand, A novel method for deriving the diffraction transfer matrix and its application to multi-body interactions in water waves, Ocean Engineering 94 (2015) 173–185.
[49] N. Faedo, S. Olaya, J. V. Ringwood, Optimal control, MPC and MPC-like algorithms for wave energy systems: An overview, IFAC Journal of Systems and Control 1 (2017) 37–56.
[50] R. Genest, J. V. Ringwood, A critical comparison of model-predictive and pseudospectral control for wave energy devices, Journal of Ocean Engineering and Marine Energy 2 (2016) 485–499.
[51] D. Garcia-Violini, J. V. Ringwood, Energy maximising robust control for spectral and pseudospectral methods with application to wave energy systems, International

Journal of Control 94 (4) (2021) 1102–1113.
[52] D. García-Violini, M. Farajvand, C. Windt, V. Grazioso, J. V. Ringwood, Passivity considerations in robust spectral-based controllers for wave energy converters, in: 2021 XIX Workshop on Information Processing and Control (RPIC), IEEE, 2021, pp. 1–6.
[53] G. Bacelli, J. V. Ringwood, Numerical optimal control of wave energy converters, IEEE Transactions on Sustainable Energy 6 (2) (2015) 294–302.
[54] T. Stehly, P. Beiter, P. Duffy, 2019 cost of wind energy review, Tech. rep., NREL, USA (12 2020).
[55] S. Barstow, G. Mørk, D. Mollison, J. Cruz, The wave energy resource, in: Ocean Wave Energy, Springer, 2008, pp. 93–132.
[56] A. Ulazia, M. Penalba, G. Ibarra-Berastegui, J. Ringwood, J. Saénz, Wave energy trends over the Bay of Biscay and the consequences for wave energy converters, Energy 141 (2017) 624–634.
[57] A. Zarketa-astigarraga, M. Agirre-aspiazu, A. Martinmayor, K. Castro, M. Martinez-agirre, B. De Miguel, M. Penalba, Air turbine Optimisation for OWC Wave Energy Converters : Sensitivity of Realistic Wave Climates, in: 15th European Wave and Tidal Energy Conference, no. September, Bilbao, Spain, 2023, p. 493. doi:10.36688/ewtec-2023-493.
URL https://doi.org/10.36688/ewtec-2023-493
[58] S. Weller, D. N. Parish, D. Trnroos, L. Johanning, Open sea OWC motions and mooring loads monitoring at BiMEP, in: Proceedings of the 12th European Wave and Tidal Energy Conference., no. August, Cork, Ireland, 2017, pp. 1 –10.
[59] A. A. Carrelhas, L. M. Gato, J. C. Henriques, A. F. Falcão, J. Varandas, Test results of a 30 kW self-rectifying biradial air turbine-generator prototype, Renewable and Sustainable Energy Reviews 109 (2019) 187–198.
[60] A. F. O. Falcão, Wave energy utilization: A review of the technologies, Renewable and Sustainable Energy Reviews 14 (3) (2010) 899–918.
[61] D. T. Gaebele, M. E. Magaña, T. K. A. Brekken, O. Sawodny, State space model of an array of oscillating water column wave energy converters with inter-body hydrodynamic coupling, Ocean Engineering 195 (November 2019) (2020) 106668. doi:10.1016/j.oceaneng.2019.106668.
URL https://doi.org/10.1016/j.oceaneng.2019.106668
[62] P. Thies, L. Johanning, P. Mcevoy, A novel mooring tether for peak load mitigation: Initial performance and service simulation testing, International Journal of Marine Energy 7 (07 2014). doi:10.1016/j.ijome.2014.06.001.
[63] F. Khalid, A. Rhahida, L. Johanning, B. de Miguel, D. Tornroos, P. Goodwin, Mooring open-sea operating data analysis, Tech. Rep. OPERA project D2.2, University of Exeter (2019).
URL http://opera-h2020.eu/wp-content/uploads/2019/09/OPERA_D2.2_Mooring-open-sea-data-analysis_UNEXE_20190621_v1.2.pdf
[64] T. Bloise Thomaz, D. Crooks, E. Medina-Lopez, L. van Velzen, H. Jeffrey, J. Lopez Mendia, R. Rodriguez Arias, P. Ruiz Minguela, O&m models for ocean energy converters: Calibrating through real sea data, Energies 12 (13) (2019). doi:10.3390/en12132475.
URL https://www.mdpi.com/1996-1073/12/13/2475
[65] K. Xu, K. Larsen, Y. Shao, M. Zhang, Z. Gao, T. Moan, Design and comparative analysis of alternative mooring systems for floating wind turbines in shallow water with emphasis on ultimate limit state design, Ocean Engineering 219 (2021) 108377.
[66] I. Touzon, V. Nava, B. de Miguel, V. Petuya, A comparison of numerical approaches for the design of mooring systems for wave energy converters, Journal of Marine Science and Engineering 8 (7) (2020) 523.